Six-band k·p calculation of spin-dependent interband tunneling in strained broken-gap heterostructures under a quantizing magnetic field

A. Zakharova
Institute of Physics and Technology of the Russian Academy of Sciences, Nakhimovskii Avenue 34, Moscow 117218, Russia

K. Nilsson and K. A. Chao
FTT, Department of Physics, Lund University, Sölvegatan 14A, S-223 62 Lund, Sweden

S. T. Yen
Department of Electronics Engineering, National Chiao Tung University, Hsinchu, Taiwan, Republic of China
(Received 14 January 2005; revised manuscript received 1 August 2005; published 22 September 2005)

We investigate spin-dependent interband magnetotunneling processes in strained broken-gap resonant tunneling structures made from InAs, AlSb, and GaSb, which are promising materials for quantum devices. InAs/AlSb/GaSb/InAs/AlSb/GaSb double-barrier structures grown on both InAs and GaSb are considered. Transmission coefficients for interband tunneling processes from individual eigenstates in the InAs emitter as well as current-voltage characteristics were calculated using a six-band **k·p** model and the scattering matrix method. We predict that due to lattice-mismatch induced strain, the interband tunneling current density for the structure grown on InAs can be one or two orders of magnitude less than that for the structure grown on GaSb. Furthermore, as a consequence of interband magnetotunneling, structures grown on different substrates yield different spin polarization of the tunneling current. It is obtained that the current spin polarization can be greater than 90%. These resonant tunneling structures can be used as spin filters in the rapidly growing field of spintronics.

DOI: 10.1103/PhysRevB.72.115329 PACS number(s): 73.40.Gk, 73.40.Kp

I. INTRODUCTION

In InAs/AlSb/GaSb broken-gap heterostructures, the InAs conduction band overlaps with the GaSb valence band, resulting in electrons tunneling from the InAs conduction band into the GaSb valence band through the AlSb barrier. Such interband tunneling structures have been studied extensively in the last 15 years both experimentally[1–9] and theoretically using realistic models which take the coupling of electron, light-hole, and heavy-hole states into account.[10–19] These structures exhibit negative differential resistance (NDR) with high values of peak-to-valley current ratio (PVCR) and peak current density. Hence they are promising for device applications. While both single- and double-barrier structures show NDR in current-voltage (*I-V*) curves, the PVCRs are usually higher for double-barrier structures. Unusually high PVCRs were observed in the InAs/AlSb/GaSb/AlSb/InAs resonant tunneling structure (RTS) Ref. 1 and in the InAs/AlSb/GaSb/InAs/AlSb/GaSb RTS.[7] In the latter case, conduction band electrons of the InAs emitter tunnel through hybridized electron-hole quasibound levels in the GaSb/InAs quantum well into valence band states of the GaSb collector.

Multiple NDR structures are observed in RTS with an InAs quantum well[5] and with a GaSb quantum well[6] when an external magnetic field is applied perpendicular to the interfaces. Such an applied field creates Landau levels in the contact layers as well as in the quantum well. The theoretical calculation[15] on magnetotunneling for the InAs/AlSb/GaSb/AlSb/InAs RTS which has neglected the lattice-mismatch induced strain and the band bending effect, has suggested that this multiple NDR structure originates from interband tunneling through quasibound states of different Landau levels. The problem becomes more interesting after the recent discovery that the lattice-mismatch induced strain considerably changes the subband dispersions[20] and the Landau-level structures[21] in the GaSb/InAs quantum well.

Moreover, the tunneling and the resonant tunneling of electrons and holes in structures of zinc-blende materials are spin dependent even in the absence of magnetic fields. Theoretical investigations suggest that this dependence is caused by the spin-orbit interaction and structural asymmetry (including the asymmetry due to an applied bias)[22–27] or bulk inversion asymmetry.[18,27,28] However, in nonmagnetic structures in the absence of magnetic fields the tunneling probabilities for spin-up and spin-down states with opposite in-plane wave vectors are equal due to time reversal symmetry. To obtain a spin polarization of the tunneling current, it has been proposed to utilize an electric field parallel to the heterointerface creating an asymmetry of the quasiparticle distribution function in the emitter.[24,26,27] Hence, these devices can be used as spin filters—the sources of spin-polarized currents of electrons or holes.[29] If a magnetic field is present, a tunnel current with a spin polarization can be achieved without the need of an asymmetric distribution function. With a magnetic field applied perpendicular to the interfaces, all levels are spin split due to the Zeeman effect. Such an advantage was used to fabricate a spin filter on an intraband RTS with a dilute magnetic semiconductor quantum well.[29,30] The resulting large electron *g* factor in the well material allows one to achieve a spin polarization of the cur-

rent up to 60% (Ref. 29). Also, a ferromagnetic semiconductor can be used as an emitter[31,32] or as a quantum well[19] to provide spin polarization of the tunnel current. Spin polarizations as large as 80% was obtained experimentally in the Esaki tunnel diode with a (GaMn)As *p*-type emitter,[32] and a spin current polarization as high as 90% was predicted for an interband broken-gap RTS with a GaMnSb quantum well in the absence of magnetic fields.[19] In this paper we investigate spin-dependent interband magnetotunneling in a nonmagnetic RTS with a GaSb/InAs quantum well. Such a structure can be useful for fabrication of spin filters due to the large electron *g* factor in the well resulting from hybridization of electron and hole levels.[21,33] Since it is important to obtain a current with spin polarizations of different signs,[29] we consider strained RTS grown on both InAs and GaSb.

The typical InAs/AlSb/GaSb/InAs/AlSb/GaSb RTS has a *n*-type InAs emitter layer and a *p*-type GaSb collector layer. Such a structure was investigated experimentally in the absence of magnetic fields.[7] In the past we have studied energy level structures in the InAs/GaSb quantum wells with the scattering matrix method[20,21,34] and interband magnetotunneling through a GaSb quantum well with the transfer matrix method[15] using multi band models, which include mixing of conduction band states, light-hole states, and heavy-hole states. However, our earlier calculation on interband magnetotunneling[15] has neglected lattice-mismatch induced strain, bulk anisotropy of the quasiparticle spectrum, and band bending effects. In this paper, with a semiself-consistent calculation, these important effects are taken into account in our model Hamiltonian to be outlined in Sec. II The precise meaning of semiself-consistent calculation will be explained later when we solve simultaneously the Schrödinger equation and the Poisson equation. We then investigate the interband magnetotunneling through hybridized electron-hole Landau levels in the GaSb/InAs quantum well with the scattering matrix method, and arrive at some very complicated transmission coefficient spectra which will be analyzed in Sec. III. Using these transmission coefficient spectra to calculate the interband magnetotunneling current in Sec. IV, we discover that the spin polarization of the tunneling current can be controlled with the sample structure. The obtained spin polarization values of the current are greater than 90%. Consequently, this RTS can work as a spin filter. Section V briefly summarizes the present work.

II. MODEL HAMILTONIAN AND METHOD

The system to be studied in this work is the InAs/AlSb/GaSb/InAs/AlSb/GaSb double-barrier RTS. The growth direction is [001] which we choose as the *z* axis. The *x* axis is along the [100] direction, and the *y* axis is along [010]. The flat energy band profile in the absence of strain is shown in Fig. 1 with solid lines for the conduction band edge $E_C(z)$ and dashed lines for the valence band edge $E_V(z)$. We use the six-band $\mathbf{k}\cdot\mathbf{p}$ Hamiltonian $\hat{H}$, which can be expressed symbolically as a 6×6 matrix operator

$$\hat{H} = \hat{H}_K + \hat{H}_Z + \hat{H}_\epsilon. \tag{1}$$

The first matrix operator $\hat{H}_K$ depends on the band edges $E_C(z)$ and $E_V(z)$, the modified Luttinger parameters, the canonical momentum operators, and the interband momentum matrix elements. The operator $\hat{H}_Z$ is the Zeeman term for an applied magnetic field *B* along the *z* axis. It is convenient to represent these matrix operators using the following sets of basis functions: electron states $|s_{1/2,\pm 1/2}\rangle$, light-hole states $|p_{3/2,\pm 1/2}\rangle$, and heavy-hole states $|p_{3/2,\pm 3/2}\rangle$. These six states are ordered as $|s_{1/2,1/2}\rangle, |p_{3/2,1/2}\rangle, |p_{3/2,3/2}\rangle, |s_{1/2,-1/2}\rangle, |p_{3/2,-1/2}\rangle$, and $|p_{3/2,-3/2}\rangle$. The first three states are the spin-up states and the other are the spin-down states. The explicit expressions of the matrix elements $\hat{H}_K+\hat{H}_Z$ are very complicated and can be found in Ref. 15 where the effect of band state mixing on interband magnetotunneling is studied. In writing down the matrix representations, the linear-in-*k* terms and Kane's *B* parameter, resulting from the lack of inversion symmetry in bulk zinc-blende crystals, are neglected because their contributions to the final results are very small.

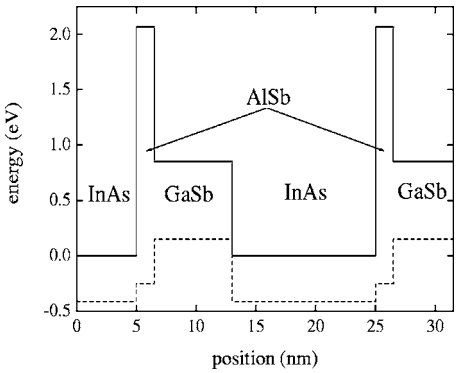

FIG. 1. Conduction band edge (solid lines) and valence band edge (dashed lines) profiles of the InAs/AlSb/GaSb/InAs/AlSb/GaSb RTS under flat-band conditions.

The Landau level structures in the AlSb/GaSb/InAs/AlSb quantum well and the contact layers are influenced by the lattice-mismatch induced strain, which is represented by the operator $\hat{H}_\epsilon$ in Eq. (1). In terms of the basis functions listed above, the matrix representation of the operator $\hat{H}_\epsilon$ was given in Ref. 21 where it was found that strain plays the essential role in the observed semimetal-semiconductor transition in broken-gap heterostructures. Here we should also point out that $\hat{H}_\epsilon$ excludes the negligibly small interband deformation potential terms and the spin-orbit interaction terms.

With $\hat{H}$ well defined, the multicomponent envelope function $\psi=(\psi_1\psi_2\psi_3\psi_4\psi_5\psi_6)^T$ for the whole structure and the corresponding eigenenergy *E* satisfy the equation

$$\hat{H}\psi = E\psi. \tag{2}$$

By taking proper boundary conditions at the interfaces and neglecting the warping terms in the Hamiltonian, this equation is solved with the scattering matrix method.[21] Transmission coefficients and the tunneling current density are calculated in a way similar to that used in Ref. 15. However, in the present work we will solve the Schrödinger equation and the Poisson equation semiself-consistently with the charge accu-

mulation in the quantum well neglected. That is, our calculation includes the band bending in the contacts but not in the quantum well. We will discuss the accuracy of this semiself-consistent scheme later when we present the numerical results. At each iteration the procedure of solving Eq. (2) remains the same. Here we will outline the characteristic features of the eigenstates as well as the computation procedure for the interband tunneling.

A magnetic field applied perpendicular to the interfaces creates Landau levels in both contacts and in the quantum well, where the spatial confinement produces a series of subbands. Hence, each spatially quantized subband in the well splits into a number of spin-polarized Landau levels. Each of these levels can be constructed in terms of InAs and GaSb bulk states. The bulk states are characterized by a quantum number n, which ranges from -2 to infinity.[15,21] The multicomponent envelope function $\psi^{(n)}$ for the bulk state corresponding to quantum number n can be expressed as

$$\psi^{(n)} = \boldsymbol{d}\exp(ik_y y + ik_z z), \tag{3}$$

where k_y and k_z are wave vector components. In terms of the harmonic oscillator functions $f_\nu(x')$ for the Landau-level ν and the argument $x' = x - \hbar c k_y/(|e|B)$, the six components vector function has the form

$$\boldsymbol{d} = \begin{pmatrix} C_1 f_n(x') \\ C_2 f_n(x') \\ C_3 f_{n-1}(x') \\ C_4 f_{n+1}(x') \\ C_5 f_{n+1}(x') \\ C_6 f_{n+2}(x') \end{pmatrix}. \tag{4}$$

When we use the method described in Ref. 15 to derive the coefficients C_i and the wave vector component k_z for a given energy E, we must take into account the bulk anisotropy resulting from the difference between the Luttinger parameters γ_2 and γ_3. Since the total wave function is $\bar{\psi} = \Sigma_i u_i \psi_i$, where the u_i's are the basis functions, electron states and hole states of different Landau-level indices ν and spins s can mix in each bulk state. The quantum number n coincides with the Landau-level index of the spin-up electron state which contributes to the total wave function $\bar{\psi}$. The number of mixed states depends on the quantum number n, because $f_\nu(x') = 0$ if $\nu < 0$.

We will briefly discuss the character of these states. Let $s > 0$ be the spin parallel to the applied field, and $s < 0$ antiparallel to the field. In each bulk state with $n \geqslant 1$, electron states and light-hole states with $[\nu = n; s > 0]$ and $[\nu = n+1; s < 0]$ mix to heavy-hole states with $[\nu = n-1; s = -1/2]$ and $[\nu = n+2; s = 1/2]$. For a bulk state with $n = -2$, the only contributions to the wave function are from the $[\nu = 0; s = -1/2]$ heavy-hole states. For a bulk state with $n = -1$, there are contributions from both electron and light-hole states with $[\nu = 0; s < 0]$, as well as from heavy-hole states with $[\nu = 1; s = -1/2]$. Finally, a bulk state with $n = 0$ contains electron and light-hole states with $[\nu = 0; s > 0]$ and $[\nu = 1; s < 0]$, and heavy-hole states with $[\nu = 2; s = -1/2]$. For given energy and k_y, the number m of bulk states is 4 for each $n \geqslant 1$ and for both the forward and the backward waves. For $n = 0, -1$ and -2, the value of m is 3, 2, and 1, respectively. The bulk states in the InAs conduction band are electronlike and are characterized by Landau-level index ν with either $s = 1/2$ or $s = -1/2$, because the main contribution to their multicomponent envelope function is either ψ_1 or ψ_4 corresponding to the s-type basis functions.

Since the boundary conditions are satisfied for each quantum number n separately,[21] we can solve Eq. (2) for each n. Due to the boundary conditions, at the heterostructure interfaces all bulk states of a given quantum number n mix. Because of these mixing it is possible for electrons in the conduction band states in the InAs emitter to perform interband tunneling with changing Landau-level index and spin orientation.[15] Furthermore, in the GaSb/InAs quantum well, states from different subbands but with the same quantum number n also mix, resulting in anticrossings in the Landau-level structures.[21,33] All these features are important to the magnetotunneling as will be discussed later.

We will approximate the potential profile derived from the Poisson equation by a step wise constant function, and then employ the scattering matrix method to derive the transmission coefficients as in Ref. 21. In each sublayer ℓ, the envelope function is expressed as a linear combination of all forward and backward bulk states for a given energy E, wave vector component k_y, and quantum number n

$$\boldsymbol{\psi} = \exp(ik_y y)\sum_{j=1}^{m}\left[a_j^{(\ell)}\exp[ik_{z,j}^{(\ell)}(z - z_{\ell-1})]\mathbf{d}_+^{(\ell)} + b_j^{(\ell)}\exp[-ik_{z,j}^{(\ell)}(z - z_\ell)]\mathbf{d}_{-j}^{(\ell)}\right], \tag{5}$$

where $z_{\ell-1}$ and z_ℓ are the z coordinates of the left and right boundaries of the ℓth layer. The vectors $\mathbf{d}_{\pm j}^{(\ell)}$ are the column vectors given by Eq. (4) corresponding to the jth forward and backward bulk states in the ℓth sublayer, respectively. The coefficients $a_j^{(\ell)}, b_j^{(\ell)}$ and $a_j^{(k)}, b_j^{(k)}$ for the different sublayers ℓ and k are connected by the $(2m)\times(2m)$ scattering matrix $S(\ell, k)$ as[21]

$$\begin{pmatrix} \mathbf{a}^{(k)} \\ \mathbf{b}^{(\ell)} \end{pmatrix} = S(\ell, k)\begin{pmatrix} \mathbf{a}^{(\ell)} \\ \mathbf{b}^{(k)} \end{pmatrix}. \tag{6}$$

The sublayer in the InAs emitter near the barrier is chosen as the first sublayer, and the sublayer in the GaSb collector near the barrier is the Nth sublayer. For the incident state j, we set $a_i^{(1)} = \delta_{i,j}$ and $\mathbf{b}^{(N)} = 0$. Then Eq. (6) with $\ell = 1$ and $k = N$ gives the solutions for the wave functions of all transmitted waves in the collector. The transmission coefficient $T_{ri}(E)$ for interband tunneling from the incident state i with energy E into the transmitted state r is given by[15]

$$T_{ri}(E) = \left(\int dx j_{zr}\right)/\left(\int dx j_{zi}\right), \tag{7}$$

where j_{zi} is the incident probability current density and j_{zr} the transmitted one. The probability current density j_z is calculated from its corresponding 6×6 matrix operator $\hat{j}_z = (1/\hbar)(\partial\hat{H}/\partial\hat{k}_z)$ as

$$j_z = \mathrm{Re}(\psi^\dagger \hat{j}_z \psi). \quad (8)$$

Finally, under the applied bias V_t the electric current density $j(V_t)=\Sigma_{r,i} j_{ri}(V_t)$ is obtained from

$$j_{ri}(V_t) = \frac{|e|^2 B}{(2\pi)^2 \hbar^2 c} \int dE\, T_{ri}(E)[f(E) - f(E + |e|V_t)], \quad (9)$$

where $f(E)$ is the Fermi-Dirac distribution function.

For the incident i (or transmitted r) state we will use i_+ (or r_+) to label the state with spin $s>0$, and i_- (or r_-) with spin $s<0$. Then the spin polarizations of the current in the emitter $P_e(V_t)$ and in the collector $P_c(V_t)$ are defined as[19,26,27]

$$P_e(V_t) = \left(\sum_{r,i_+} j_{ri_+}(V_t) - \sum_{r,i_-} j_{ri_-}(V_t) \right) / j(V_t), \quad (10)$$

$$P_c(V_t) = \left(\sum_{r_+,i} j_{r_+i}(V_t) - \sum_{r_-,i} j_{r_-i}(V_t) \right) / j(V_t). \quad (11)$$

The quantities $P_e(V_t)$ and $P_c(V_t)$ characterize the spin filtering efficiency, and will be calculated as functions of applied bias. Due to spin-flip tunneling processes, $P_e(V_t)$ can differ from $P_c(V_t)$.

III. MAGNETOTUNNELING UNDER FLAT-BAND CONDITIONS

The system we will investigate is an InAs/AlSb/GaSb/InAs/AlSb/GaSb RTS, with 1.5 nm width AlSb barriers and a quantum well consisting of a 6.5 nm thick GaSb layer and a 12 nm thick InAs layer. Under flat-band conditions the band-edge profile of the system is shown in Fig. 1 Such a type of structure grown on GaSb with thicker 3 nm AlSb barriers was studied experimentally in the absence of magnetic fields.[7] Here we reduce the AlSb barrier width in order to avoid inconveniently long computation time. For numerical calculation we need many material parameters. The values of energy gaps, split-off energies, interband momentum matrix elements, conduction and valence band offsets, and lattice constants are found in Ref. 35. The deformation potentials and the stiffness constants are available in Ref. 36.

It is important to point out that the RTS can be grown on either an InAs substrate or a GaSb substrate. For these two cases, because the strain effects are different, the energy level structures in the GaSb/InAs quantum well and the transmission coefficients are also different. Hence, different growth conditions lead to different potential distributions in the sample. To illustrate the general properties of the RTS, we will first present our results for the RTS under flat-band conditions. That is, the effect of band bending due to charge accumulation is not considered yet.

Energy level structures, calculated using our model, are shown in Fig. 2 with panel (a) for the structure grown on an InAs substrate, and panel (b) for the one on a GaSb substrate. These will help us to understand the magnetotunneling. In both panels (a) and (b), solid curves are for $n=-2$, dashed curves for $n=-1$, dotted curves for $n=0$, and dashed-dotted curves for $n=1$. At zero magnetic field, there are four subbands which are labeled as $1e$ for the first electron subband, $1\ell h$ for the first light-hole subband, $1hh$ for the first heavy-hole subband, and $2hh$ for the second heavy-hole subband. Several energy gaps produced by anticrossings are visible in each panel. Because of the anticrossings, the character of the subbands may change with the magnetic field. These results are qualitatively similar to those in Ref. 21, where the relevant mechanisms to produce such complicated energy level structures were discussed in depth. It is important to notice that the peak positions of the transmission coefficients correspond to the positions of the quasibound Landau levels.

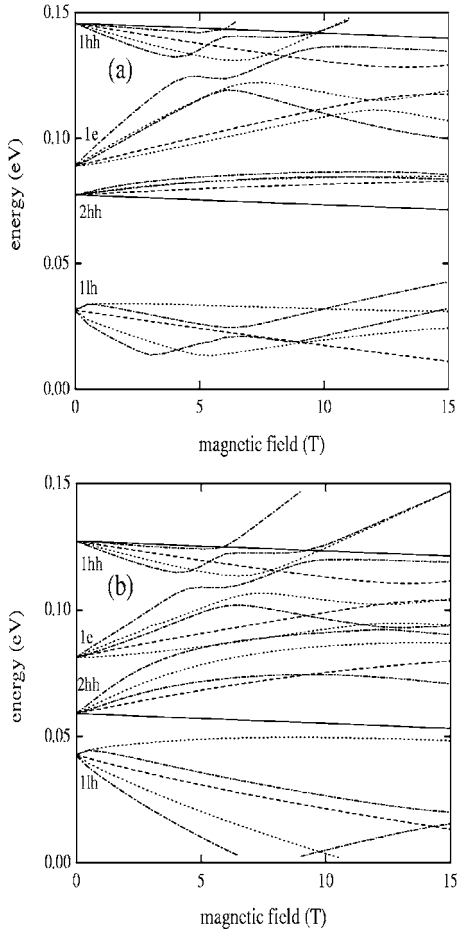

FIG. 2. Flat-band Landau-level structures of the InAs/AlSb/GaSb/InAs/AlSb/GaSb RTS grown on (a) InAs and (b) GaSb. The conduction band edge of unstrained InAs is used as energy reference. The solid curves are for $n=-2$, dashed curves for $n=-1$, dotted curves for $n=0$, and dashed-dotted curves for $n=1$.

Since states with different quantum numbers n do not mix, the transmission coefficient for individual n's can be calculated separately. To illustrate the dependence of tunneling on the sample fabrication process, the transmission coefficients at a magnetic field $B=15$ T are shown in Fig. 3 for a RTS grown on InAs, and in Fig. 4 for a RTS grown on GaSb. In both figures, panel (a) is for $n=-1$, panel (b) for $n=0$, and panel (c) for $n=1$. Panels (a) show interband tunneling from the $[\nu=0; s=-1/2]$ electron states in the InAs emitter into all hole states in the GaSb collector. In panels (b), solid curves show interband tunneling from the $[\nu=0; s=1/2]$

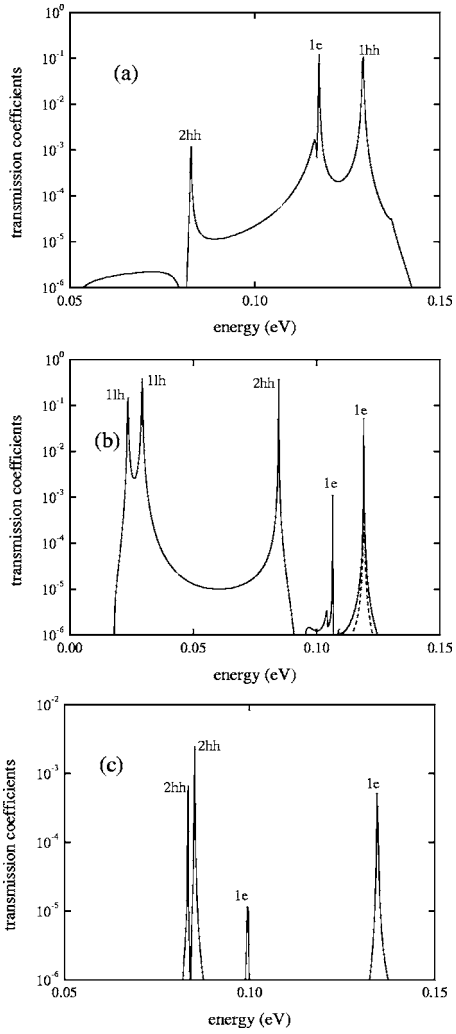

FIG. 3. Flat-band transmission coefficients spectra of the InAs/AlSb/GaSb/InAs/AlSb/GaSb RTS grown on InAs, under an applied magnetic field of 15 T. Panel (a) is for $n=-1$, panel (b) for $n=0$, and panel (c) for $n=1$. The initial state of the tunneling is $[\nu=0;s=-1/2]$ for the curves in panel (a) and $[\nu=1,s=1/2]$ for the curves in panel (c). In panel (b) the initial state of the tunneling processes is $[\nu=0;s=1/2]$ for the solid curves, and $[\nu=1;s=-1/2]$ for the dashed curves.

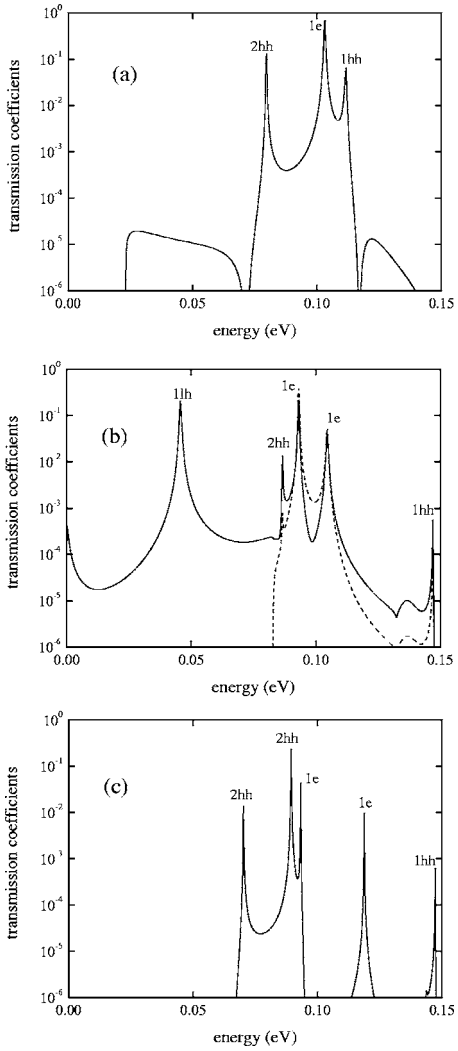

FIG. 4. Flat-band transmission coefficients spectra of the InAs/AlSb/GaSb/InAs/AlSb/GaSb RTS grown on GaSb, under an applied magnetic field of 15 T. Panel (a) is for $n=-1$, panel (b) for $n=0$, and panel (c) for $n=1$. The tunneling processes represented by these curves are the same as those in Fig. 3.

electron states into all hole states, while dashed curves show interband tunneling from the $[\nu=1;s=-1/2]$ electron states into all hole states. Finally, the curves in panels (c) show interband tunneling from the $[\nu=1,s=1/2]$ electron states to all hole states.

The peaks of the transmission coefficient curves of the resonant magnetotunneling are identified and labeled with the information given in Fig. 2. Since there are four subbands in the quantum well through which interband tunneling can occur, there are four types of resonant tunneling in Figs. 3 and 4 for $n=-1,n=0$, and $n=1$. The states of the $1hh$ and $2hh$ subbands with $n=-2$ do not mix with other states, and hence interband tunneling through them cannot occur. Also, under a magnetic field of 15 T interband tunneling from the electron Landau states in the InAs emitter with $n>1$ is forbidden by the selection rule.

We notice that in Fig. 2 each of the $1e$ and $1\ell h$ states with $n=0$ and $n=1$, as well as each of the $1hh$ and $2hh$ states with $n=1$ splits into two states with opposite spins due to the formation of different Landau levels and the Zeeman effect. This Zeeman split produces the double resonant tunneling peaks in panels (b) and (c) of Figs. 3 and 4. In panels (b) the higher energy $1e$ resonances result from interband tunneling through electronlike Landau levels in the well, while the lower energy $1e$ resonances correspond to interband resonant tunneling through heavy-holelike levels. In panels (c), the $1e$ resonances also result from interband tunneling through heavy-holelike Landau levels in the well. The situation is somewhat different for $1\ell h$ states with $n=0$. Since, as indicated in Fig. 2, the splitting of this level is much smaller for the structure grown on InAs rather than on GaSb, there are two peaks in Fig. 3(b) for the $1\ell h$ transmission coefficients, but only one in Fig. 4(b). One should notice that the magnitude of all transmission coefficients is much smaller in panel (c) of Fig. 3 for the case $n=1$.

On the contrary, there is no split of resonance peaks in neither Fig. 3(a) nor in Fig. 4(a) for $n=-1$. Instead, at a high field of 15 T, the $1hh$ levels become electronlike while the $1e$ levels become heavy-holelike. However, due to the strong mixing of electron and hole states, electronlike resonances are weaker than heavy-holelike resonances.

IV. *I-V* CHARACTERISTICS AND CURRENT SPIN POLARIZATION

To pass a current through a sample, the doped contacts serve as a source and a drain. We set the donor concentration in the InAs contact at 2×10^{17} cm^{-3}, and the acceptor concentration in the GaSb contact at 5×10^{18} cm^{-3}. The Fermi level E_F is measured from the InAs conduction band edge near the left AlSb barrier. Depending on the substrate on which the RTS is grown, E_F at zero bias has different values: $E_F=66$ meV for an InAs substrate, and $E_F=80$ meV for a GaSb substrate.

The previous sections describe the way to calculate the transmission coefficients for a given potential function. Knowing the transmission coefficients from the source to the drain, the electric current and the related spin polarization can be derived with Eqs. (9)–(11). To perform such calculations, we need to know the spatial distribution of carriers, which also modifies the potential function through the Poisson equation. Under an applied magnetic field, a full self-consistent calculation is extremely complicated. Therefore, we will first perform a full self-consistent calculation in the absence of the applied field.

The main effect of charge accumulation in the quantum well is to shift the energy level positions and consequently shift the positions of the resonant tunneling peaks. This effect becomes increasingly important when we increase the thickness of the InAs and/or the GaSb layer in the InAs/GaSb quantum well. There exists a relevant investigation[37] on a RTS where the quantum well consists of a 30 nm thick n-doped InAs layer of donor concentration 2×10^{11} cm^{-2}, and a 15 nm thick undoped GaSb layer. It was found that, in the absence of an external magnetic field, the self-consistent corrections to the energy level positions can be as large as 25 meV. However, for the sample studied in our present work, in the quantum well the InAs layer is only 12 nm thick and the GaSb layer 6.5 nm. For such a narrower quantum well, our calculated self-consistent corrections of the energy levels in the well are about 5 meV at zero bias, if the donor concentration in the InAs layer of the well is 3×10^{11} cm^{-2} and the acceptor concentration in the GaSb layer is 1.5×10^{11} cm^{-2}. While a finite bias voltage can modify the potential profile across the quantum well between the AlSb barriers, the external electric field is screened by the carriers in the well. This results in a redistribution of local electric field among the AlSb barriers and the quantum well. The effect of this redistribution on the energy levels in the quantum well is not significant and does not enhance the self-consistent correction considerably, because the barriers are very thin.

When an external magnetic field is applied along the growth direction (z axis), although the energy level structure in the well becomes very complicated, the self-consistent correction is expected to change only slightly. Therefore, similar to the tunneling processes for the case of no external magnetic field, the magnetotunneling through our sample of the narrow quantum well should not be modified qualitatively by the charge accumulation in the well. Under such a consideration, instead of full self-consistency, our numerical results of magnetotunneling current and its spin polarization are calculated semiself-consistently.

The phenomena which are investigated in the present work can be observed only at low temperatures such that the thermal energy k_BT is much less than all characteristic energies of the system. Under the experimental situation of high magnetic field, the temperature should be very low. Therefore it is not unreasonable to perform our numerical calculation at zero temperature. Let us first set the magnetic field to 15 T to demonstrate our findings unambiguously. The so-obtained *I-V* curves are shown in Fig. 5 with panel (a) for a RTS grown on InAs and panel (b) for a RTS grown on GaSb. The total current which is shown as solid curves in panels (a) and (b) has two tunneling contributions from states in the emitter with different values of n,ν, and s. The dashed curves are for $[n=0,\nu=0,s=1/2]$, and the dotted curves are for $[n=-1,\nu=0,s=-1/2]$. Because the $1\ell h$ levels are much lower than all states occupied by holes in the GaSb collector, interband tunnelings occur mainly through $1hh$, $1e$, and $2hh$ levels. In connection to the transmission coefficients shown in Figs. 3 and 4, the dotted curve in Fig. 5(a) is related to the solid curve in Fig. 3(a), and the dashed curve in Fig. 5(b) is associated with the solid curve in Fig. 4(b).

For a RTS grown on GaSb substrate, the spin components of the current density in the collector can differ significantly from those in the emitter. We illustrate this feature in Fig. 5(b) where the dashed-dotted curve is for $s>0$ component while the dashed-dotted-dotted curve is for the $s<0$ component. Furthermore, we demonstrate the effects of strain and bulk anisotropy with Fig. 5(c): If we neglect the strain, the total current is represented by the solid curve, which becomes the dashed curve when the bulk anisotropy is also ignored.

The current peaks in Fig. 5 are connected to the multiple peaks of the transmission coefficients. The number of current peaks is one in panel (a), two in panel (b), but five in panel (c) for the solid curve of unstrained structure. When the bulk anisotropy is ignored, this number is reduced as shown in Fig. 5(c). The spin-dependent contributions to the total current in Fig. 5 clearly indicate that in the RTS grown on InAs the electron tunneling current is dominated by the $s=-1/2$ component, while in the RTS grown on GaSb the $s=1/2$ component is dominant. The origin of this difference is the variation of the Landau level positions in the well and the magnitudes of the tunneling resonances caused by the lattice-mismatch induced strain. In the high energy region in Fig. 3, there are two high peaks in panel (a) due to the tunneling through $1e$ and $1hh$ states, while in panel (b) the two $1e$ peaks are substantially lower. Hence, in the RTS grown on InAs, interband tunneling from electron states in the emitter with $[\nu=0,s=-1/2]$ through $1e$ and $1hh$ levels for $n=-1$ is the main contribution to the current density. On the other hand, the difference in peak magnitude in panels (a) and

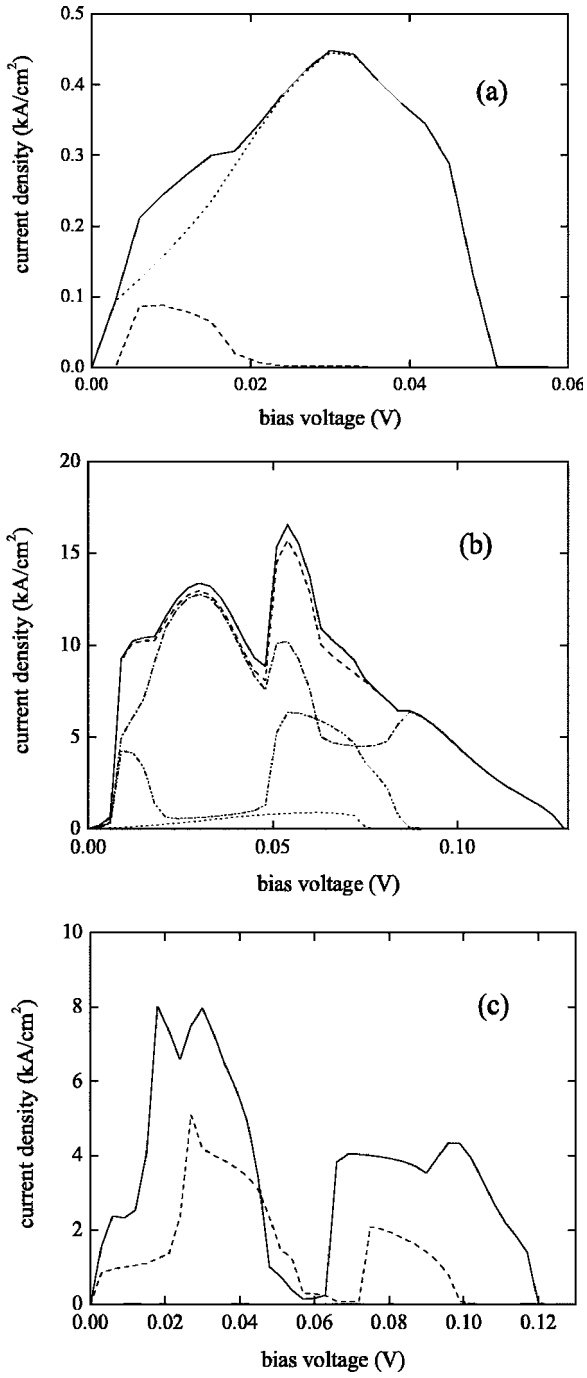

FIG. 5. Current-voltage characteristics of the InAs/AlSb/GaSb/InAs/AlSb/GaSb RTS grown on (a) InAs, (b) GaSb. The applied magnetic field is 15 T. In panels (a) and (b), the solid curves are for the total current density, the dashed curves are the partial tunneling current from states in the emitter with $[n=0,\nu=0,s=1/2]$, and the dotted curves are from states with $[n=-1,\nu=0,s=-1/2]$. In panel (b), the dashed-dotted curve represents the $s>0$ component of the current density in the collector, while the dashed-dotted-dotted curve represents the $s<0$ component. For comparison, panel (c) shows the *I-V* curves of an unstrained RTS. The solid curve is the total current density when the strain is neglected, and when the bulk anisotropy is also neglected the total current density becomes the dashed curve.

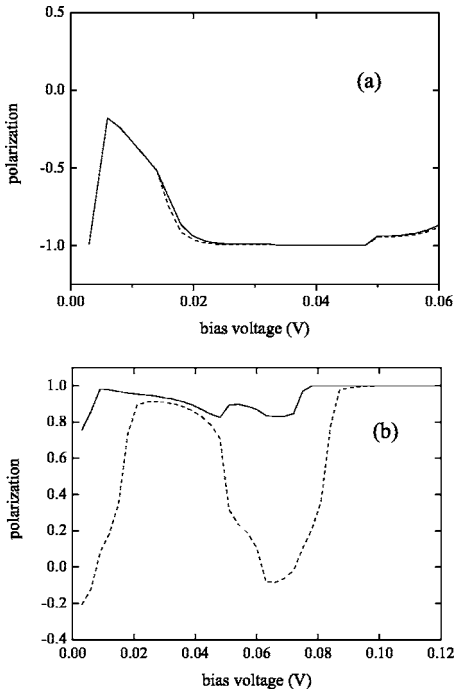

FIG. 6. Spin polarization of the current in the emitter (solid curves) and in the collector (dashed curves) versus applied bias. In panel (a) the RTS is grown on InAs and in panel (b) on GaSb.

(b) of Fig. 4 is not large. In this structure grown on GaSb, tunneling from states with $[\nu=0,s=1/2]$ is dominant because the concentration of electrons in the InAs emitter with $[\nu=0,s=1/2]$ is larger. In this respect, our RTS can work as a spin filter.

It is interesting to notice that in Fig. 5 the current density in panel (a) for the structure grown on InAs is at least one order of magnitude less than that in panel (b) for the structure grown on GaSb. One of the reasons lies in the fact that in the structure grown on InAs, the valence band edge of the strained GaSb layer is split. In this case, without an external magnetic field, the heavy-hole band edge is higher than the light-hole band edge by 0.048 eV. Therefore, holes mainly occupy heavy-hole states in the GaSb collector of the RTS grown on InAs. The tunneling probabilities into heavy-hole states are usually less than those into light-hole states, causing smaller current density in a RTS grown on InAs. The smaller total tunneling current in the RTS grown on InAs is a combined effect of the different transmission coefficient profiles and the different percentages of light-holes in the GaSb collector. A similar effect in InAs/AlSb/GaSb single-barrier structures was observed experimentally[3,4] in the absence of an applied magnetic field. However, the difference in the magnitudes of current density in RTS grown on different substrates is much larger for the case of high magnetic field. The reason is a stronger decrease of light-hole concentration in the GaSb contact layer of the RTS grown on InAs due to the formation of Landau levels.

The spin polarizations of the current P_e in the emitter and P_c in the collector, calculated from Eqs. (10) and (11) under a field strength of 15 T, are shown in Fig. 6 for the RTS grown on InAs [panel (a)] and on GaSb [panel (b)]. The solid

curves are for P_e, and the dashed curves are for P_c. Since the spin-flip processes are not important in the structure grown on InAs, we see in panel (a) that $P_e \simeq P_c$. It is important to notice that this spin polarization is negative and can reach 100% for bias voltage $V_t > 0.02$ V.

On the other hand, spin-flip processes in the RTS grown on GaSb can result in a considerable difference between P_e and P_c. However, the magnitude of this difference depends on the applied bias voltage as can be seen in Fig. 6(b). In the regions $0.02 < V_t < 0.05$ V and $V_t > 0.09$ V, P_e and P_c have almost the same positive value. Especially for $V_t > 0.09$ V, the polarizations are nearly 100%. While P_e remains always positive, in two regions of bias voltage, P_c can be negative, and this negative spin polarization of the collector current can reach 20% at low bias voltage. Consequently, the RTS grown on GaSb can be used as a voltage-controlled spin filter which was also proposed by other authors.[19,30]

In a RTS grown on GaSb, the spin polarization of the current can be varied by adjusting the impurity concentration. As an illustrating example, we have increased the donor concentration in the InAs emitter to about 10^{18} cm^{-3}. Although the theoretical analysis becomes much more complicated in this case because more Landau levels contribute to the interband tunneling, our calculation yields a maximum value of 90% negative spin polarization of the collector current, without an essential decrease of the maximum value of positive spin polarization. These calculated characteristics of our proposed spin filters are much better than those observed experimentally for the RTS with a dilute magnetic semiconductor quantum well[29,30] and for the Esaki tunnel diode with a ferromagnetic semiconductor emitter.[31,32]

While our numerical analysis was performed with a very high magnetic field of 15 T in order to clearly demonstrate the interesting phenomena, it is important to point out that because of the reduction of the Zeeman spin splitting of the Landau levels, the values of P_e and P_c may decrease when the magnetic field is lowered. We have performed further calculations to investigate this field effect, and found that nevertheless the maximum values of P_e and P_c at $B=7$ T can be nearly 100%, and the sign of the spin polarization of the current in the emitter (but not in the collector) can be switched by varying the bias voltage if the RTS is grown on GaSb. As a conclusion, the spin polarization in such broken-gap systems as well as its switching sign can exist in a large range of magnetic field strength, and can be optimized by changing the sample structure, the doping profile, and the applied bias voltage.

V. SUMMARY

The broken-gap heterostructures are very complicated electron systems, and all published works emphasize specific effects and phenomena although the starting Hamiltonians are very similar. The main topics which have been studied so far are electronic structures and tunneling transport with or without an external magnetic field. Reference 15 gives the interband magnetotunneling calculations without lattice-mismatch induced strain, while Ref. 21 presents Landau-level structures in a strained InAs/GaSb quantum well. In the present work we combine the key issues of these two papers, and perform a complicated calculation on spin-dependent interband magnetotunneling through hybridized electron-hole Landau levels in the quantum well under an applied magnetic field $B=15$ T. In our calculation we also include effects of bulk anisotropy of the quasiparticle spectra and band bending in contacts (but not in the well).

We have resolved the complicated interband magnetotunneling processes in great detail. We have presented a clear physical picture for different spin-polarized interband tunneling currents in a RTS grown on different substrates resulting from multiple peaks of the transmission spectra. We have predicted that the difference between the current density magnitudes for RTS grown on InAs and GaSb at $B=15$ T is much greater than that observed experimentally for the case of zero magnetic field. We have found that in the RTS grown on InAs the spin polarization of the tunneling electrons in the emitter is $s=-1/2$, while in the RTS grown on GaSb this spin polarization is $s=1/2$. The spin polarization of the current in the emitter results in spin polarization of the current in the collector, which is negative for the structure grown on InAs and can change sign for the structure grown on GaSb. We have obtained positive spin polarizations of the emitter and collector currents about 100% in RTS grown on GaSb and negative spin polarizations of the emitter and collector currents about 100% in RTS grown on InAs. Consequently, the InAs/AlSb/GaSb/InAs/AlSb/GaSb broken-gap heterostructures can be used as efficient spin filters in the rapidly growing field of spintronics.

ACKNOWLEDGMENTS

This work was financially supported by the Nordic Academy for Advanced Study Research Network Programmer, the NSC of ROC under Grant No. 91-2215-E-009-058 and the RFBR under Grant No. 03-02-16788.

[1] J. R. Söderström, D. H. Chow, and T. C. McGill, Appl. Phys. Lett. **55**, 1094 (1989).

[2] L. F. Luo, R. Beresford, and W. I. Wang, Appl. Phys. Lett. **55**, 2023 (1989).

[3] R. Beresford, L. F. Luo, K. F. Longenbach, and W. I. Wang, Appl. Phys. Lett. **56**, 952 (1990).

[4] J. F. Chen, L. Yang, M. C. Wu, S. N. G. Chu, and A.Y. Cho, J. Appl. Phys. **68**, 3451 (1990).

[5] E. E. Mendez, H. Ohno, L. Esaki, and W. I. Wang, Phys. Rev. B **43**, 5196 (1991).

[6] E. E. Mendez, H. Ohno, L. Esaki, and W.I. Wang, in *Resonant Tunneling in Semiconductors, Physics and Applications, NATO Advanced Studies Instituted Series B: Physics* edited by L. L. Chang, E. E. Mendez, and C. Tejedor. (Plenum, New york,

1991), Vol. **277**, p.51.
[7] Y.-H. Wang, M. H. Liu, M. P. Houng, J. F. Chen, and A. Y. Cho, IEEE Trans. Electron Devices **41**, 1734 (1994).
[8] R. R. Marquardt, D. A. Collins, Y. X. Liu, D. Z.-Y. Ting, and T. C. McGill, Phys. Rev. B **53**, 13624 (1996).
[9] E. M. Gonzalez, Y. Lin, and E. E. Mendez, Phys. Rev. B **63**, 033308 (2000).
[10] D. Z.-Y. Ting, E. T. Yu, and T. C. McGill, Phys. Rev. B **45**, 3583 (1992).
[11] M. S. Kiledjian, J. N. Schulman, K. L. Wang, and K. V. Rousseau, Phys. Rev. B **46**, 16012 (1992).
[12] M. A. Davidovich, E. V. Anda, C. Tejedor, and G. Platero, Phys. Rev. B **47**, 4475 (1993).
[13] Y. X. Liu, R. R. Marquardt, D. Z.-Y. Ting, and T. C. McGill, Phys. Rev. B **55**, 7073 (1997).
[14] J. Genoe, K. Fobelets, C. Van Hoof, and G. Borghs, Phys. Rev. B **52**, 14025 (1995).
[15] A. Zakharova and K. A. Chao, J. Phys.: Condens. Matter **14**, 5003 (2002).
[16] I. Lapushkin, A. Zakharova, V. Gergel, H. Goronkin, and S. Tehrani, J. Appl. Phys. **82**, 2421 (1997).
[17] A. Zakharova, Semicond. Sci. Technol. **13**, 569 (1998).
[18] A. E. Botha and M. R. Singh, Phys. Rev. B **67**, 195334 (2003).
[19] I. Vurgaftman and J. R. Meyer, Phys. Rev. B **67**, 125209 (2003).
[20] A. Zakharova, S. T. Yen, and K. A. Chao, Phys. Rev. B **66**, 085312 (2002).
[21] A. Zakharova, S. T. Yen, and K. A. Chao, Phys. Rev. B **69**, 115319 (2004).
[22] CalvinYi-Ping Chao and S. L. Chuang, Phys. Rev. B **43**, 7027 (1991).
[23] F. T. Vasko, Sov. Phys. JETP **73**, 352 (1991).
[24] A. Zakharova, F. T. Vasko, and V. Ryzhii, J. Phys.: Condens. Matter **6**, 7537 (1994).
[25] A. Voskoboynikov, S. S. Liu, and C. P. Lee, Phys. Rev. B **58**, 15397 (1998).
[26] A. Voskoboynikov, S. S. Liu, C. P. Lee, and O. Tretyak, J. Appl. Phys. **87**, 387 (2000).
[27] David Z.-Y. Ting and X. Cartoixa, Phys. Rev. B **68**, 235320 (2003).
[28] V. I. Perel', S. A. Tarasenko, I. N. Yassievich, S. D. Ganichev, V. V. Bel'kov, and W. Prettl, Phys. Rev. B **67**, 201304(R) (2003).
[29] G. Schmidt, J. Phys. D **38**, R107 (2005).
[30] A. Slobodskyy, C. Gould, T. Slobodskyy, C. R. Becker, G. Schmidt, and L. W. Molenkamp, Phys. Rev. Lett. **90**, 246601 (2003).
[31] M. Kohda, Y. Ohno, Y. Takamura, F. Matsukora, and H. Ohno, Jpn. J. Appl. Phys., Part 2 **40**, L1274 (2001).
[32] P. Van Dorpe, Z. Liu, W. Van Roy, V. F. Motanyi, M. Sawicki, G. Borghs, and J. De Boeck, Appl. Phys. Lett. **84**, 3495 (2004).
[33] S.-F. Tsay, J.-C. Chiang, Z. M. Chau, and I. Lo, Phys. Rev. B **56**, 13242 (1997).
[34] A. Zakharova, S. T. Yen, and K. A. Chao, Phys. Rev. B **64**, 235332 (2001).
[35] E. Halvorsen, Y. Galperin, and K. A. Chao, Phys. Rev. B **61**, 16743 (2000).
[36] M. P. C. M. Krijn, Semicond. Sci. Technol. **6**, 27 (1991).
[37] I. Lapushkin, A. Zakharova, S. T. Yen, and K. A. Chao, J. Phys.: Condens. Matter **16**, 4677 (2004).